Semiempirical modified embedded-atom potentials for silicon and germanium

M. I. Baskes, J. S. Nelson, and A. F. Wright*
Theoretical Division, Sandia National Laboratories, Livermore, California 94551-0969
(Received 24 April 1989)

Semiempirical potentials for silicon, germanium, and their alloys are derived with use of the modified-embedded-atom-method formalism. Following Baskes [Phys. Rev. Lett. **59**, 2666 (1987)], it is found that the host electron density which is a linear superposition of atomic densities in the embedded-atom method (EAM) must have an angular modification in order to properly describe the bond-bending forces in the diamond-cubic structure. The angular dependence of this host electron density was found to be in qualitative agreement with the density of a first-principles calculation. As in the EAM, the potential functions are determined by using the measured lattice constants, sublimation energies, elastic constants, and alloying energies of silicon and germanium. In addition, first-principles calculations of structural energies are used. The potentials are used to calculate the energetics and geometrics of point defects, surfaces, metastable structures, and small clusters. In all cases, the calculations have been compared to first-principles calculations and experiment when available. The calculations predict that the vacancy mechanism is the dominant diffusion mechanism in both silicon and germanium. Surface energies and relaxations of the low-index faces of Si and Ge are compared with first-principles calculations.

I. INTRODUCTION

The past few years have resulted in a number of new semiempirical and empirical models for covalent materials.[1-8] Development of these models has occurred in part because of the intense interest in development of semiconductor devices. Investigators have realized that simple pair-potential models or valence-force potentials are not sufficiently accurate to predict structural properties far from the reference structure to which they were fitted. In addition, they have found that *ab initio* methods require too much computer time to calculate large-scale structures or phenomena. Hence a large effort has been expended in the development of computationally efficient empirical models that have predictive value away from the configuration space in which they were fitted.

We have recently developed one of the above-mentioned semiempirical models. Our motivation for developing yet again another model is twofold. First, we feel it is important to have a model with some physical basis so that extrapolation to untested geometries or alloys can be made with some confidence. Secondly, all of the above models work well for some problems, but fail miserably for others. Our hope is to develop a more universal model capable of describing many phenomena. In the development of this model, which we call the modified embedded-atom method (MEAM), we have extended our previously developed embedded-atom method[9] (EAM) in an *ad hoc* manner to include the differences between metallic and covalent bonding. The EAM has been used quite successfully in predicting numerous properties of metals and alloys, e.g., defects,[10,11] liquids,[12] surface structure[9,10] and reconstruction,[13] segregation[14] and phase stability[15] in alloys, mechanical properties including dislocation mobility and fracture,[16] bulk and surface phonons,[17] interface structures and strength,[18] and hydrogen on surfaces.[19]

In the EAM (Ref. 9) the energy of a cluster of atoms, $E_{\rm tot}$, is given by the expression

$$E_{\rm tot}=\sum_i F_i(\rho_{h,i})+\tfrac{1}{2}\sum_{\substack{i,j\\(i\neq j)}}\phi_{ij}(R_{ij})\ , \tag{1}$$

where $\rho_{h,i}$ is the total electron density at atom i associated with the host (i.e., the rest of the atoms in the system), F_i is the energy to embed an atom i into this density, and ϕ_{ij} is a pair-potential term representing electrostatic interactions between atoms i and j separated by a distance R_{ij}.

We have modified the EAM previously[7] to include the bond-bending forces inherent in a covalent material. As discussed in detail below, the modification occurs in the way in which the host electron density $\rho_{h,i}$ is calculated. In the EAM the host electron density is given by a linear superposition of spherically averaged atomic densities. This ansatz has been found to work quite well for fcc transition-metal elements with almost full d shells. For the case of materials with directional bonding, this procedure will be shown to lead to elastic constants that are inconsistent with experiment. Thus we modify the expression for the host electron density by including angle-dependent contributions.

The purpose of this paper is threefold: First, to expand on the MEAM, giving more details about its implementation, correcting an error in Ref. 7 in the elastic-constant calculation, and presenting the generalization of the MEAM to multicomponent systems; second, to present a set of functions that are applicable to Si and Ge, and their alloys; and third, to apply these functions to

numerous calculations that may be compared to experiment and *ab initio* calculations. The format of the paper follows this plan. Section II states the model, shows how the functions are derived, and compares the model predictions to the data base to which it was fitted. Section III presents the predictions of the energies and geometries of point defects, metastable structural energies, geometries and elastic constants, surface structures and energies, cluster stability, and electron-density profiles. These results are compared to experiment and *ab initio* calculations whenever possible. The final section summarizes our results.

II. MODEL

A. First-neighbor model (FNEAM)

The motivation of the model has been given previously[7] but will be repeated and expanded here for completeness. Our objective is to obtain the energy of a configuration of atoms as a function of their nuclear positions. Let us start with the formulation of the EAM for a homogeneous monatomic solid in which only first-neighbor interactions are considered. In this case, the energy of each atom in the solid is identical and, from Eq. (1), depends upon the nearest-neighbor distance, r, by the relationship

$$E(r)=F(n\rho^a(r))+0.5n\phi(r) , \tag{2}$$

where n is the number of first neighbors in the structure under consideration, ρ^a the spherically averaged atomic electron density at a distance r from the nucleus, ϕ the pair interaction, and F the embedding function. Note that the host atomic density to which each atom is subjected is identical and assumed equal to $n\rho^a$, the superposition of the densities of its neighbors. This density is used as the argument of the embedding function.

We now consider a reference structure, e.g., the diamond-cubic structure where we have n_1 first nearest neighbors. For the case of a uniform expansion or contraction, Rose *et al.*[20] have shown that the energy per atom may be described by a universal function, E_r:

$$E_r(a^*)=-E_0(1+a^*)e^{-a^*} , \tag{3}$$

where the scaled distance a^* is given by

$$a^*=\beta(r-r_1) , \tag{4a}$$

$$\beta=\left[\frac{9B\Omega_0}{r_1^2E_0}\right]^{1/2} , \tag{4b}$$

and E_0 is the sublimination energy, r_1 is the equilibrium first-neighbor distance, B is the bulk modulus, and Ω_0 $[=(\sqrt{4/3}r_1)^3$ for the diamond structure] is the equilibrium atomic volume. These quantities are for the reference structure.

We now equate Eqs. (2) and (3) applied to the reference structure and solve for the pair potential ϕ:

$$\phi(r)=\frac{2}{n_1}[E_r(a^*(r))-F(n_1\rho^a(r))] . \tag{5}$$

Hence, by using experimental quantities from a reference structure, we have determined a pair potential that we will now use in a general structure. That is, it is now possible to calculate the energy of a solid, E_n, in various crystal structures having n nearest neighbors. By inserting Eq. (5) into Eq. (2) we obtain

$$E_n=\frac{n}{n_1}E_r(a^*)+F(n\rho^a)-\frac{n}{n_1}F(n_1\rho^a) . \tag{6}$$

Note that this expression depends on both reference structure properties as well as the coordination in the structure of interest.

Previously,[7] we have shown that a specific form for the embedding energy yields the same logarithmic relationship between the bond length and number of bonds that has been noted by Pauling.[21] Using this form,

$$F(\rho)=E_0\frac{\rho}{\bar{\rho}}\ln\left[\frac{\rho}{\bar{\rho}}\right] , \tag{7}$$

where $\bar{\rho}=n_1\rho^a(r_1)$ is the host density at equilibrium in the reference structure, i.e., the structure with n_1 neighbors, Eq. (6) becomes

$$E_n=\frac{n}{n_1}E_r(a^*)+E_0\frac{n\rho^a}{\bar{\rho}}\ln\left[\frac{n}{n_1}\right] . \tag{8}$$

To find the equilibrium nearest-neighbor distance we set the derivative of E_n with respect to r equal to zero,

$$\frac{\partial E_n}{\partial r}=0=\frac{n}{n_1}E_r'(a^*)\beta+\frac{E_0n(\rho^a)'}{\bar{\rho}}\ln\left[\frac{n}{n_1}\right] , \tag{9a}$$

and to first order in the difference in the number of nearest neighbors,

$$r-r_1\cong\frac{-\rho^a(r_1)'}{\beta^2\rho^a(r_1)}\ln\left[\frac{n}{n_1}\right] . \tag{9b}$$

The minimum energy for n neighbors, E_n^0, is obtained by expanding Eq. (8) to second order in $r-r_1$ and inserting Eq. (9b). This operation yields

$$\ln\left[\frac{E_n^0}{-E_0}\right]\cong-\frac{1}{2}\left[1-\left[\frac{-\rho^a(r_1)'}{\beta\rho^a(r_1)}\right]^2\right]\left[\ln\left[\frac{n}{n_1}\right]\right]^2 . \tag{10}$$

Let us now compare the FNEAM model with the structural energies and geometries from first-principles calculations. In order to do this we need as input the experimental values of E_0, B, and r_1. These numbers are given in Table I. The remainder of Table I will be discussed below. In addition, we need the ratio $\rho^a(r_1)'/\rho^a(r_1)$, which we take as a free parameter which is used to fit the energy differences of the metastable phases relative to the diamond structure from the first-principles calculations.[25,26] The value obtained for this parameter is -1.9 Å^{-1}.

Figure 1 shows the predicted change in the equilibrium first-neighbor distance for silicon as a function of coordination. The approximate solution, Eq. (9b), is shown as

TABLE I. Values of the parameters used in the EAM models. Units are eV for energy, eV/Å^3 for the elastic constant, and Å for distance.

Experimental data			MEAM		
	Si	Ge		Si	Ge
E_0	4.63[a]	3.85[a]	α_i	3.20	3.52
B	0.610[b]	0.469[b]	m_i	4	6
r_1	2.351[c]	2.450[c]	a_i^1	0.60	0.73
			a_i^2	0.87	1.12
			ρ_i^0	1.0	0.91
			A_{ij}	0.986	
			r_c	5.0	5.0
			δ	0.5	0.5

[a]Reference 22.
[b]Reference 23.
[c]Reference 24.

the solid line, while the exact solution to Eq. (9a) is shown by the solid symbols. For comparison the local-density-approximation (LDA) calculations of Yin and Cohen[25] and the quantum-chemical (QC) calculations of Ho *et al.* and Melius[26] are shown. The relative coordination n/n_1 is given by the inverse of the bond order for the QC calculations. For the case of the triple bond, a linear HSi—SiH molecule is used. This configuration is unstable, but best represents the bonding that would occur in a triple bond. The agreement between the FNEAM model and the first-principles calculations is quite good. Also, the approximate Eq. (9b) adequately represents the solution of Eq. (9a). In Fig. 2 the predicted minimum energies versus coordination are shown. The solid line denotes the approximate relationship of Eq. (10), while the solid symbols are from the exact Eq. (8). Again the approximation is shown to be good. Also shown in Fig. 2 are the energies calculated using LDA.[25] The LDA energy has been shifted by a constant to agree with the experimental silicon sublimation energy. The agreement with the FNEAM model is not as good as for bond distance, but certainly shows the correct decrease in energy with increased coordination.

We show in Fig. 3 the pair potential which results using a density given by a simple exponential with $\rho^a(r_1)'/\rho^a(r_1) = -1.9$ Å^{-1} as above. We cut off the interaction discontinuously at 3 Å to limit the range to first neighbors. More informative is the effective pair potential discussed previously by Foiles,[12] given to lowest order by

$$\psi(r) = \phi(r) + 2F'(\rho^*)\rho^a(r) \ . \tag{11}$$

The effective pair potential depends on environment

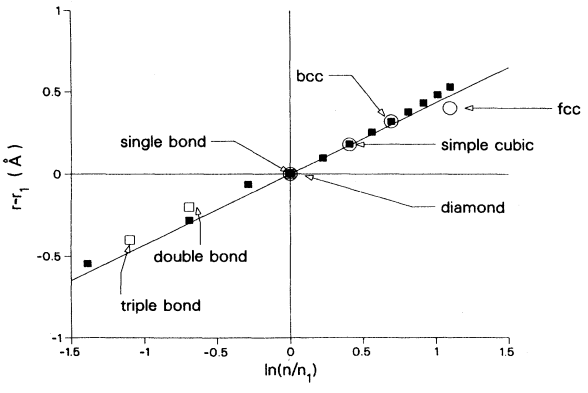

FIG. 1. First-neighbor equilibrium bond distance for silicon (relative to the diamond structure) as a function of coordination. Open symbols indicate first-principles calculations, circles the LDA (Ref. 24) calculations, and squares QC (Ref. 25) calculations, while the solid symbols represent the exact FNEAM predictions. The solid line is the approximate solution for the FNEAM model. The free parameter in the FNEAM model, $\rho^a(r_1)'/\rho^a(r_1)$, was used to fit the first-principles calculations and resulted in a value of -1.9 Å^{-1}.

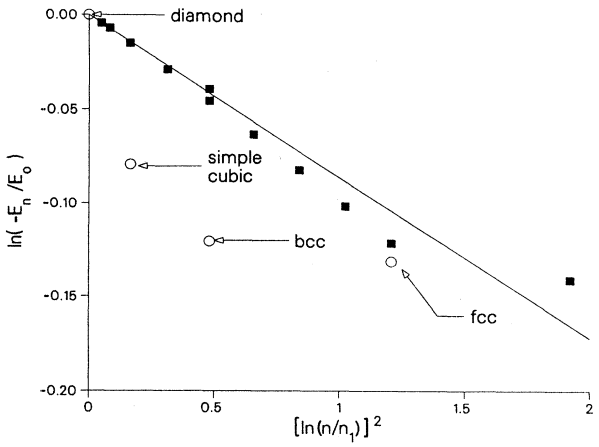

FIG. 2. Energy per atom for silicon (relative to the diamond structure) as a function of coordination. Open symbols indicate first-principles calculations, while the line represents the approximate FNEAM predictions. The solid symbols represent the exact solution for the FNEAM model. The free parameter in the FNEAM model, $\rho^a(r_1)'/\rho^a(r_1)$, was taken as -1.9 Å^{-1} as in Fig. 1.

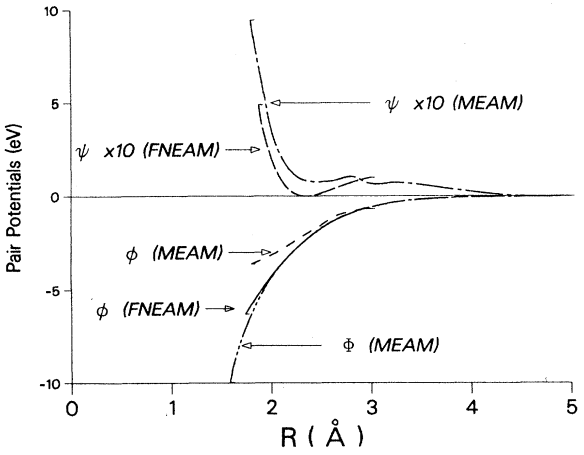

FIG. 3. Pair-potential interactions used for silicon in the FNEAM and MEAM models. The potentials are discussed in the text.

through ρ^*, the density that an atom "sees." For the embedding function of Eq. (7) we get

$$\psi(r)=\frac{2}{n_1}\left\{E_r(a^*)-E_0\frac{\rho^a(r)}{\rho^a(r_1)}\left[\ln\left[\frac{\rho^a(r)}{\rho^a(r_1)}\right]-1\right]\right\} \quad (12)$$

for an atom at the equilibrium position in the diamond structure, i.e., $\rho^*=\bar{\rho}$. Note that the effective pair potential has a minimum at the first-neighbor distance and is qualitatively similar to the simple pair potentials previously used for metals.

The major problems with the FNEAM model as presented above are related to the elastic shear constants. (We incorrectly calculated C_{44} in Ref. 7. The details of the correct method of calculation are given in Appendix A.) The predicted shear constants for the FNEAM are compared to the experimental values[23] in Table II. Note that the FNEAM does not agree at all with experiment. In fact, as expected for a first-neighbor central-potential model, $\gamma'=0$, in obvious disagreement with experiment. This problem, however, is relatively simple to fix. By inclusion of more neighbors in the EAM, the experimental values of C_{11} and C_{12} may be fitted exactly. We will demonstrate this below.

A more serious problem occurs when we look at the Cauchy discrepancy, $\Delta C=C_{12}-C_{44}$ (see Table II). The experimental value for silicon as well as germanium is negative. This negative value is a direct result of the directionality of bonding in these semiconducting materials, which strongly influences the bond bending forces. In contrast, the metals which we have previously modeled with the EAM all have positive Cauchy discrepancies. This difference is critical, as the EAM formalism (see Ref. 9) predicts the sign of the Cauchy discrepancy to be the same as the sign of the second derivative of the embedding function (at $\bar{\rho}$). The embedding function we have chosen to use [Eq. (7)] has a positive curvature; hence it is impossible to fit the elastic constants of Si or Ge with the EAM formalism presented above. However, it is not difficult to include the effects of bond-bending forces, as shown in the following section.

B. Modified EAM (MEAM)

The FNEAM has two flaws: interactions further than first neighbors, and bond-bending forces need to be included. Let us now recast the model to include these two effects.

The total energy of the solid is given by the usual EAM expression [Eq. (1)] with a modified host electron density, $\rho_{h,i}$. We include in the host electron density an angle-dependent term that results in bond-bending forces. The specific angular dependence chosen for this term vanishes in ideal cubic structures. The angular dependence may be considered as the first two terms in an expansion of spherical harmonics as used by Biswas and Hamann, or as an expansion in gradients of the density.[27] The modified electron density is given by

$$\rho_{h,i}=\sum_{j\,(\neq i)}\rho_j^a(R_{ij})+\sum_{\substack{j\,(\neq i)\\ k\,(\neq i)}}[a_j^1a_k^1\cos\theta_{jik}-a_j^2a_k^2(1-3\cos^2\theta_{jik})]\rho_j^a(R_{ij})\rho_k^a(R_{ik})\,, \quad (13)$$

where we have specifically indicated that the atomic density ρ_j^a depends on the type of atom j, θ_{jik} is the included angle between atoms j, i, and k with atom i the central atom, and the $a_i^{1,2}$ are constants depending on the atom type i. The product form for the $a_i^{1,2}$ is chosen arbitrarily and this choice merits more study to assess whether or not its form is important. Note that in the previous paper, where we considered a monatomic solid, the constant $a=(a_i^2)^2$ and $a_i^1=0$. We will see below that $a_i^1\neq 0$ when we calculate C_{44} correctly (see Appendix A). In Eq. (13) the first summation is the usual linear superposition of atomic densities, while the double summation is the angular modification. Note that the $j=k$ term (a pair interaction) in this summation *is* included. The angle-dependent term must decrease in magnitude as either bond length of the three atoms ij or ik increases. The natural scaling for this decrease is the atomic electron density. By symmetry atoms j and k should be treated equivalently; hence we postulate that the distance dependence should be a function of the product of the atomic densities of atoms j and k at atom i. The simplest function is the one chosen in Eq. (13). [In the gradient expansion, ρ' rather than ρ should be used; however, for the exponential density used below, ρ' is approximately proportional to ρ and Eq. (13) is still appropriate.]

We now calculate the like-atom pair-potential term in the MEAM in a manner analogous to that used above in the FNEAM. As above, the energy per atom of a mona-

TABLE II. Elastic shear constants for Si and Ge (values in eV/Å^3). Values were calculated in the FNEAM and fitted to experiment in the MEAM.

	Si			Ge	
	Expt.[a]	FNEAM	MEAM	Expt.[a]	MEAM
$\gamma=C_{44}$	0.495	0.011	0.493	0.419	0.418
$\gamma'=(C_{11}-C_{12})/2$	0.315	0	0.312	0.253	0.252
$\Delta C=C_{12}-C_{44}$	−0.095	0.610	−0.091	−0.119	−0.117

[a]Reference 23.

tomic homogeneous solid in our reference structure under uniform expansion or contraction is given by

$$E(r)=E_r(a^*)=F(\rho_i(r))+0.5n_1\Phi(r)\ , \tag{14}$$

where the total pair-potential contribution is

$$\Phi(r)=\sum_s \frac{n_s}{n_1}\phi_{ii}(a_s r) \tag{15}$$

and

$$\rho_i(r)=\sum_s n_s\rho_i^a(a_s r)\ . \tag{16}$$

In Eqs. (14)–(16), r is the first-neighbor distance and n_s is the number of neighbors at a disance $a_s r$. Note that, by construction, the angle-dependent term in Eq. (13) for the background density sums to zero for cubic structures, yielding the simple form in Eq. (16) independent of $a_i^{1,2}$. We may now solve Eq. (14) for Φ:

$$\Phi(r)=\frac{2}{n_1}[E_r(a^*)-F(\rho_i)]\ , \tag{17}$$

where E_r is obtained from Eq. (3) and F from Eq. (7). The arguments of these functions are given in Eqs. (4) and (16).

To obtain the pair potential ϕ from the total pair potential Φ requires a cutoff distance, r_c, beyond which E_r and ρ^a are zero. In this case we may solve Eq. (15) to get

$$\phi_{ii}(r)=\Phi(r)-\sum_{s\ (\neq 1)}\frac{n_s}{n_1}\Phi(a_s r)+\left[\frac{n_2}{n_1}\right]^2\Phi(a_2^2 r)\ , \quad r>\frac{r_c}{a_2 a_3}\ . \tag{18}$$

This range ($r>1.6$ Å for $r_c=5$ Å) is sufficient for most defect calculations. It is straightforward to include additional terms in Eq. (18) if one is interested in shorter distances. Alternatively, one may use a pair-interaction formalism to define ϕ at short distances, where the universal behavior [Eq. (3)] breaks down.[28]

We now have the basic equations for the MEAM. All that remains is to choose an atomic density and fit the elastic shear constants. We choose a density of the atomic form

$$\rho_i^a(r)=\rho_i^0\left[\frac{r}{r_1}\right]^{m_i}e^{-\alpha_i(r-r_1)}\ , \tag{19}$$

where we choose m_i from the appropriate atomic density for an isolated atom, but we let α_i be a free parameter rather than using the value for the isolated atom. In the formalism presented above, only density ratios appear for a single-component system. Hence the constant ρ_i^0 is arbitrary for a single-component system. When alloys are considered, the ratios of ρ_1^0 for different elements may be determined. We arbitrarily set $\rho_{\rm Si}^0$ for silicon to 1. By fitting to the shear elastic constants and the LDA calculations of metastable structures,[25] we obtain the values for $a_i^{1,2}$ and α_i shown in Table I. The cutoff distance is chosen large enough (5 Å) to be relatively unimportant. The functions E_r and ρ^a are cut off by multiplying them by the cutoff function, f_c:

$$f_c=\begin{cases}1, & r\le r_c-\delta\\ \frac{1}{2}(1+x)-\frac{5}{8}x(x^2-1)+\frac{3}{16}x(x^4-1), & r_c-\delta<r<r_c\\ 0, & r\ge r_c\end{cases} \tag{20}$$

where $x=(r_c-\delta/2-r)/(\delta/2)$. This function has vanishing first and second derivatives at $r=r_c$ and $r=r_c-\delta$.

The resultant elastic constants are compared to experiment in Table II. The agreement is quite good. Note that, in contrast to the FNEAM, the MEAM gives the correct sign of the Cauchy discrepancy. We have calculated the internal-strain parameter ζ as defined by Kleinman.[29] This parameter yields the relative sublattice displacements under the C_{44} shear. For Si (Ge) we obtain a value of $\zeta=0.74$ (0.71), in excellent agreement with the experimental values[30,31] of 0.73 (0.72). LDA calculations[32] yield values of 0.53 (0.44). The resulting pair potential, total pair potential, and the effective pair potential for silicon as defined in Eqs. (18), (17), and (11), respectively, are shown in Fig. 3. Note that the pair potential ϕ becomes equal to the total pair potential Φ at large distances when only first neighbors are important. Note also that the total pair potential is approximately equal to the pair potential for the FNEAM at distances where the FNEAM potential is defined, i.e., less than 3 Å. We may see why this is true by comparing Eqs. (5) and (17). The equations are identical if the arguments of the embedding function $(\rho/\bar{\rho})$ are equal. We have found that these functions for the FNEAM and MEAM agree to better than 10% for $0.7\le r/r_1<1.5$ and, in fact, the derivative $(\rho_i'/\bar{\rho})$ for the MEAM is equal to -1.9 Å^{-1} as in the FNEAM. We have not required this agreement; it results from our fitting of the first-principles geometries and energies. The parameters for germanium are given in Table I and results in similar functions.

In order to perform alloy calculations, we need to

TABLE III. Values (in eV) of the alloy properties used to determine the MEAM parameters. ΔE_{ZB} is the energy of ordered zinc-blende structure ($Si_{0.5}Ge_{0.5}$) relative to the separated bulk crystals, and ΔE_{do} is the energy of the disordered 50-50 alloy relative to the separated bulk crystals. LDA calculations (Ref. 35) find the ordered zinc-blende structure 0.002 eV lower in energy than the disordered 50-50 alloy.

	Expt. (LDA)	MEAM
ΔE_{do}	0.011[a]	0.013
ΔE_{ZB}	0.0093[b]	0.011

[a]Reference 34.
[b]Reference 35.

determine ρ_i^0/ρ_j^0, and $\phi_{ij}(R)$ for $i \neq j$. Previously,[9,10] we have used a geometric mean of ϕ_{ii} and ϕ_{jj} to determine ϕ_{ij}. This procedure only works for pair potentials that do not change sign. Daw[27] has shown that an arithmetic mean is also a feasible option, while Johnson[33] has proposed a density-weighted form. This latter form is given by

$$\phi_{ij}(R)=\frac{A_{ij}}{2}\left[\frac{\phi_{ii}(R)}{\rho_i^a(R)^2}+\frac{\phi_{jj}(R)}{\rho_j^a(R)^2}\right]\rho_i^a(R)\rho_j^a(R)\ . \quad (21)$$

This form (for $A_{ij}=1$) has been derived by requiring that the total energy in an alloy calculation does not change if a constant times density is added to either component's embedding function. Previously,[9] it has been noted that for a single component the addition of a constant times density to the embedding function does not change the total energy since the linear portion of the embedding function is equivalent to a pair potential. Note that Eq. (21) does not depend on ρ_i^0 and ρ_j^0 individually, but only on their ratio. We determine ρ_i^0/ρ_j^0 and A_{ij} by fitting to the experimental value[34] of the heat of formation of a random Si-Ge alloy, ΔE_{do} (do denotes disordered), and the LDA calculation[35] of the zinc-blende structure stability, ΔE_{ZB}. The resulting parameters are given in Table I and the comparison with experiment in Table III.

The model is now complete. To summarize, the total energy is calculated from Eq. (1) with the embedding energy taken from Eq. (7) and the pair potential from Eqs. (18) and (21). The host density is calculated using Eq. (13) with the atomic density taken from Eq. (19). All of the required parameters are given in Table I.

Before we proceed to use the model in the next section, we note that Appendix B contains an important computational shortcut we use to evaluate the host density. This shortcut is particularly important in the instance when we need to know energy derivatives, e.g., in energy-minimization or molecular-dynamics calculations.

III. RESULTS AND DISCUSSION

A. Point defects

The calculation of point-defect energies and geometries is an excellent test of the MEAM as numerous LDA calculations[36–39] of point defects are available for comparison. Unfortunately, the LDA calculations are accurate to only ~ 1 eV,[35,36] so only qualitative comparisons can be made. In addition, the LDA calculations show that defect energies depend strongly on charge state and Fermi level, neither of which is considered in the MEAM. The results presented here use the MEAM as formulated in Sec. II to calculate the energy and forces necessary in a conjugate gradient-minimization scheme. The number of atoms used in the simulations was increased until defect energies converged to <0.01 eV. Typically ~ 250 atoms for vacancy-type defects and ~ 1000 atoms (these calculations take only of the order of a minute on a Cray-13 computer) for interstitial-type defects were sufficient for convergence. Only the converged energies and geometries are quoted below. This energy convergence yields atom positions to better than 0.01 Å. The calculated point-defect energies and first-neighbor relaxations are given in Table IV.

All defect energies are given relative to a perfect lattice with the same total number of atoms. The predicted formation energy of a silicon vacancy, 3.19 eV, is somewhat lower than the 5–6 eV reported in LDA calculations.[36] The neutral vacancy is at the bottom of that range. The relaxation of the nearest neighbors is *towards* the vacancy, as in a metal, resulting in a lengthening of the silicon bonds of the nearest neighbors of the vacancy by 0.12 Å; this result is in disagreement with the LDA calculations,[37] which find that the nearest neighbors relax *away* from the vacancy, similar to the inward-relaxation top-layer atoms on the (111) Si surface. The interstitial-formation energies reported here are for the sixfold- (hex) coordinated position, the fourfold (T_d) position, and the

TABLE IV. Calculated point-defect energies and relaxations.

	Si		Ge	
Defect	Energy[a]	Relaxation[b]	Energy[a]	Relaxation[b]
vacancy	3.19	−0.51	5.07	−0.45
divacancy	6.00	−0.37	8.82	−0.48
vacancy SP	3.56	−0.30	5.36	−0.26
interstitial (hex)	7.07	0.33	7.14	0.34
interstitial (T_d)	4.81	0.22	5.74	0.23
interstitial (B)	5.88	1.39	7.72	1.43
interstitial (SP)	4.90	0.32	6.01	0.35

[a]In eV.
[b]First-neighbor relaxation in Å. A positive sign indicates relaxation away from the defect.

TABLE V. Calculated geometry and elastic constants of metastable phases. (Distance in Å, elastic constants in eV/Å^3, first-principles calculations in parentheses.)

	Si				Ge			
Structure	a	B	γ'	γ	a	B	γ'	γ
fcc	4.19 (3.89)[a]	1.64	0.35	0.91	4.00 (4.20)[a]	2.70	0.81	2.02
bcc	3.25 (3.09)[a]	0.11			3.35 (3.30)[a]	0.39	0.07	0.19
sc	2.61 (2.53)[a]	0.89	2.15	0.18	2.75 (2.67)[a]	0.78	1.52	0.40

[a]LDA calculation; Ref. 25.

twofold bond-centered (B) position. The relative order of stability T_d, B, hex for silicon is found to be in agreement with that found in LDA calculations for the 2+ charge state,[36] but in disagreement with the order for the neutral charge state (B, H, T_d). It is difficult to make an argument for which charge state the MEAM should be compared with. The MEAM energy predictions are in reasonable agreement with the LDA calculations,[36,37] in which the interstitial energy ranges from 5 to 7 eV depending on charge state and Fermi level. The predicted relaxations are in qualitative agreement with the LDA calculations,[36] which range from negligible for the T_d site to 0.1 Å for the hex site to 1.2 Å for the B site. Note that for Ge the relative stability order changes to T_d, hex, B. The relaxations for Ge are quite similar to those for Si.

Table IV also contains the energy of the classical saddle points (SP's) for vacancy and interstitial migration. The predicted vacancy-migration energy for Si (Ge) is 0.37 (0.29). This number agrees well with the experimental measurements of 0.33±0.03 eV for Si.[40] The self-diffusion energy in Si (Ge) for the vacancy mechanism is 3.56 (5.36) eV and for the interstitial mechanism 4.90 (6.01) eV. These numbers show that the vacancy mechanism is predicted to be the dominant self-diffusion process. The predicted activation energy compares favorably with the experimental value of 4.1–5.1 eV in silicon,[41] but poorly with the experimental value of ~3 eV in germanium.[42]

We have also calculated the activation energy for concerted exchange, i.e., a direct interchange of nearest neighbors. For silicon this process has a calculated energy of 6.56 eV to be compared with the LDA calculation[39] of 4–5 eV depending on relaxation. At the exchange SP the bond length between the two exchanging atoms is 0.03 Å less than the equilibrium bond length. For germanium this process has an activation energy of 8.32 eV and the bond length is 0.11 Å less than the equilibrium Ge bond length. This process is not competitive with vacancy diffusion.

From the divacancy energies we calculate the divacancy binding energy to be 0.38 (1.32) eV in Si (Ge). Note the large divacancy binding in germanium, which is consistent with the divacancy model used by Hirota[43] to explain his radiation-damage–recovery measurements. Hirota[43] found a value of 0.75 eV for the migration energy. For his mechanism to be operative, the divacancy binding energy must be greater than the migration energy, as we find.

B. Metastable structures

This subsection presents the results of numerous calculations of metastable structural geometries, energies, and

TABLE VI. Calculated structural properties of the noncubic metastable phases. (Distance in Å, elastic constant in eV/Å^3, first-principles calculations in parentheses.)

	Si			Ge		
Structure	a	c/a	B	a	c/a	B
β-tin	4.83 (4.83)[a]	0.62 (0.55)[a]	1.11 (0.74)[b]	4.83 (5.09)[a]	0.63 (0.55)[a]	0.81
hexagonal	2.75 (2.62)[b]	0.95 (0.93)[b]	0.90 (0.66)[b]	2.81	0.95	1.24
hcp	2.96 (2.74)[a]	1.64 (1.63)[a,c]	1.64	2.82 (2.96)[a]	1.68 (1.63)[a,c]	1.93
wurtzite	3.85 (3.86)[a]	1.62 (1.63)[a,c]	0.61	4.04 (4.04)[a]	1.54 (1.63)[b,c]	0.58

[a]LDA calculations; Ref. 25.
[b]LDA calculations; Ref. 44.
[c]c/a held fixed.

elastic constants, and compares them to LDA calculations.[25,44] As above, the MEAM formulated in Sec. II is used for the calculations. We remind the reader that only one parameter for each material, α, is used to fit all of the LDA data. The structural energies and relaxed geometries are calculated using a three-dimensional (3D) periodic array of unit cells of the structure of interest, keeping the symmetry fixed. The elastic constants are calculated by the procedure in Appendix A.

In Fig. 4 we see a comparison of the energies of various structures of Si and Ge compared to LDA calculations.[25,44] The agreement is good, usually within 0.2 eV for Si. For Ge the EAM consistently predicts less stable energetics than the LDA calculations for the structures other than diamond and wurtzite. Table V presents the predicted lattice constant and elastic constants of the cubic structures, and Table VI gives the lattice constant, c/a ratio, and bulk modulus for the noncubic phases. The agreement with LDA calculations is acceptable, with the major trends correctly predicted. Note that the shear constants for bcc Si are not given. This structure is predicted to be unstable with respect to either shear. It is interesting to note that bcc Ge is stable; however, for both bcc Si and Ge, all of the elastic constants are quite small.

In Fig. 5 we present the energy of a few structures for Si as a function of volume. In comparing the MEAM

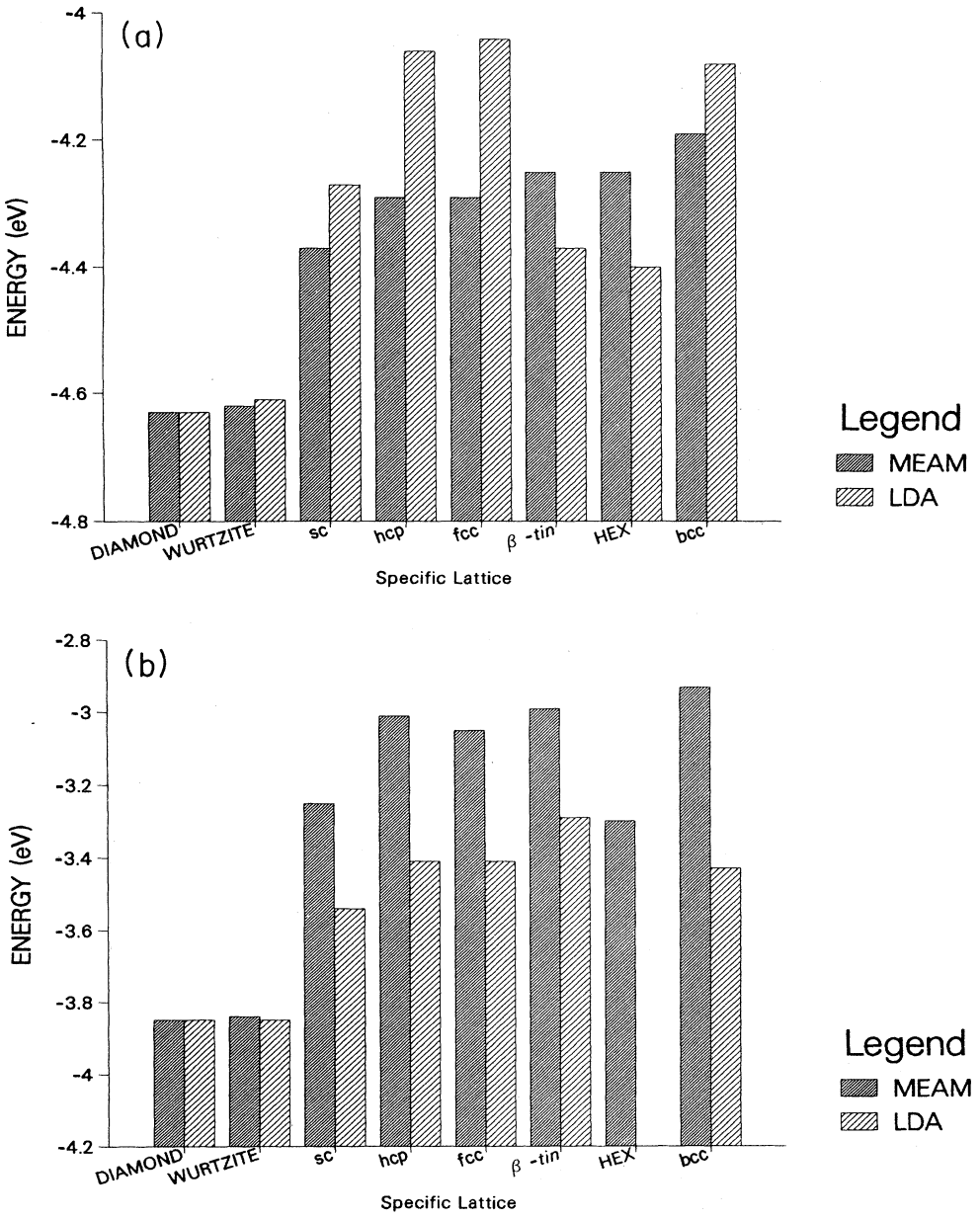

FIG. 4. Comparison of the energies of various metastable structures of (a) Si and (b) Ge with LDA calculations (Refs. 24 and 44). We could not find any calculations on the hexagonal structure of Ge.

calculations [Fig. 5(a)] with the LDA results[25] [Fig. 5(b)] we see that qualitatively the results are quite similar. The major disagreement occurs in the relative positions of the fcc and bcc curves.

We have calculated the energy of a relaxed intrinsic stacking fault in silicon in the diamond-cubic structure to be 0.077 eV/Å^2. This value is considerably higher than the LDA-calculated value[45] of 0.003 eV/Å^2. The fact that this energy is so large may be one factor leading to problems in the surface calculations below. We plan to fit to this energy in the next version of the silicon potentials, as we have often done for the fcc metals.

C. Surface structure

The calculation of surface structure, like the point defects, provides a good test for the MEAM since the bonding is modified with the generation of dangling bonds. In

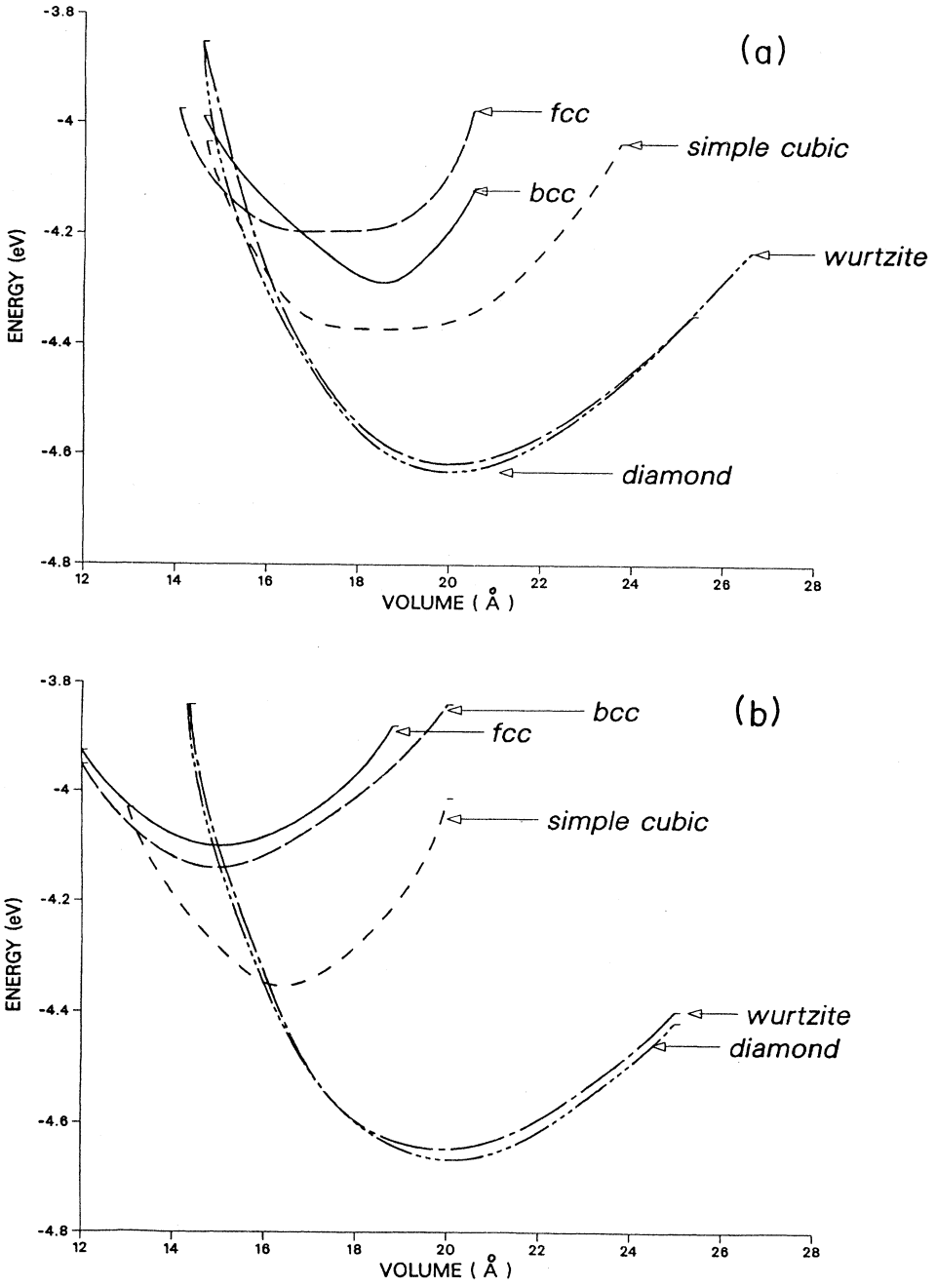

FIG. 5. Comparison of (a) MEAM and (b) LDA calculations (Ref. 24) of the energies of various structures of Si as a function of volume.

this section the atomic geometries of the Si and Ge (100), (110), and (111) surfaces will be presented. The unit cells for the three surfaces were taken to be 20–30 layers thick, which is large enough so that the surfaces are noninteracting.

The (100) surface structure of Si has been studied with a variety of empirical and first-principles interatomic potentials. Khor and Das Sarma[46] applied the empirical potentials of Stillinger and Weber,[2] Tersoff,[3] and Dodson.[4] They found that all three of these potentials give symmetric dimers with a (2×1) reconstruction. Abraham and Batra,[47] also using the Stillinger-Weber potential, found a similar (2×1) reconstruction with symmetric dimers. Pseudopotential calculations of Applebaum and Hamann[48] showed a (2×1) symmetric dimer reconstruction with significant subsurface relaxations. By allowing for asymmetric dimers, Chadi[49] showed that the surface energy could be further lowered. Yin and Cohen[50] found a reconstruction similar to Chadi,[49] with the dimer bond length shorter than the bulk bond length used by Chadi.[49] Northrup[51] has proposed a $c(4\times2)$ structure in which the second-layer atoms are dimerized and the top-layer atoms form π-bonded chains, similar to the (2×1) chain structure suggested by Pandey[52] for the (111) surface. The scanning-tunneling-microscopy (STM) studies of Tromp *et al.*[53] showed that buckled and nonbuckled dimers appear to be present in roughly equal amounts. They also observed a significant number of defects with structure similar to the π-bonded defect model of Pandey.[52] Both the experiments and the theoretical calculations suggest some sort of a (2×1) dimerized structure for Si(100) reconstruction.

The symmetry of the Ge(100) surface reconstruction seems to be well characterized experimentally. At low temperatures the surface has a $c(4\times2)$ symmetry and a (2×1) symmetry at higher temperatures.[53–56] The transition between these two phases occurs at about 150 K. Needels *et al.*,[57,58] using an *ab initio* total-energy molecular-dynamics approach, found that the $c(4\times2)$ structure with alternate buckled dimers is lowest in energy. The energy difference between the $c(4\times2)$ and (2×1) structures was found to be 0.05 eV/dimer.

The MEAM values for the (100) surface energies of Si and Ge are given in Table VII. The (2×1) symmetric dimer reconstruction is found to be the lowest-energy structure for Si, but not for Ge, although the energy difference between the (1×1) and (2×1) Ge structures is small. The Ge (2×1) structure is found to be metastable. Most of the relaxation energy for the LDA calculations[51] comes from the dimerization, and only a small amount of energy is gained by relaxation of the (1×1) surface. On the other hand, since the MEAM does not directly include dimerization, most of the energy gain is associated with relaxation of the (1×1) surface. Our calculations are consistent with the previous empirical calculations for the Si(100) surface that showed symmetric dimers.[46] One can understand why our results and the results of the other empirical calculations[46] all predict symmetric dimers. Chadi[49] has suggested that the stability of asymmetric dimers is a result of a charge transfer from the "down" to the "up" atom in the dimer. A surface band gap is produced by the lowering (raising) of the bonding (antibonding) state as a consequence of the charge transfer. The MEAM and empirical potentials do not allow for charge transfer, and therefore should always predict symmetric dimers. The atomic displacements (see Fig. 6) and interlayer distances for the lowest-energy Si and Ge (100) surfaces are given in Tables VIII and IX, respectively. The relaxations we find for the Si surface are similar to those found by Appelbaum and Hamann;[48] the main difference is the outward relaxation of the top layer predicted by the MEAM. Previous empirical potential calculations[46,47] showed an inward relaxation.

The MEAM does not give a reconstructed (110) surface for either Si or Ge. The surface energies and atomic relaxations are given in Tables X and XI, respectively. Similar to the (100) surface, the first interlayer spacing is found to be 0.24 Å (0.29 Å) larger than the bulk Si (Ge) value. In addition, the neighboring first- and second-layer chains move towards each other along the [100]

TABLE VII. Si and Ge (100) surface energies. Energies are in eV/(surface atom). The LDA results are given in parentheses.

	Si	Ge
Ideal	2.21 (2.50)[a]	2.52
(1×1)	1.81 (2.47)[a]	1.98
(2×1)	1.76 (1.72)[a]	2.00

[a]Reference 51.

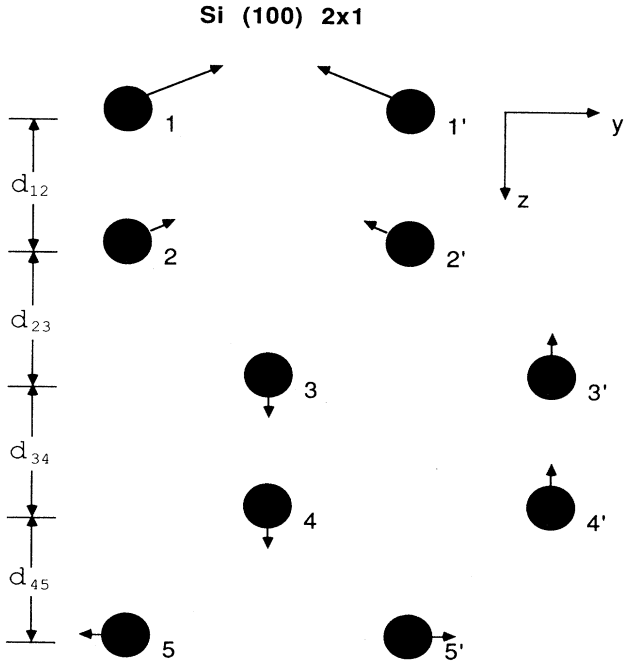

FIG. 6. Side view of the symmetric dimer reconstruction of the Si(100)-(2×1) surface as calculated with the MEAM. The arrows indicate the displacement of the atoms from their bulk-terminated positions. Atoms 1 and 1′ are in the surface layer, 2 and 2′ are second-layer atoms, etc. The values of the displacements and interlayer distances are given in Table VII.

direction by roughly 0.16 Å for both Si and Ge. The tight-binding calculations of Chadi[59] showed a (1×1) buckled surface. As mentioned above, the MEAM is not expected to give rise to buckling. STM images of the Si(110) surface[60] have indicated a (2×5) surface unit cell, which we have not investigated here.

On the (111) surface we have considered several different reconstructions: the (2×1) buckled, the (2×1) π-bonded chain,[52] and the $(n\times n)$ (for $n=3,5,7,9$) dimer stacking-fault structure.[61] The dimer-adatom stacking-fault model of Takayanagi *et al.*[62] seems to be the accepted structure of the Si(111) (7×7) reconstruction. We find that the relaxed (1×1) structure is lowest in energy [0.72 eV/(surface atom)]. The first four interlayer spacings for the (1×1) structures of Si and Ge are compared to LDA calculations[63] in Table XII. Similar to the (100) and (110) surfaces, the MEAM predicts an outward relaxation of the first interlayer separation for the (111) surface, whereas the LDA results suggest a contraction.

In Fig. 7 the surface energies for the $(n\times n)$ (for $n=3,5,7,9$) dimer stacking-fault structures are compared to the (1×1) surface energy. The surface energy is found to decrease monotonically with increasing n, but does not fall below the (1×1) surface energy. Consequently, the MEAM does not predict Si (7×7) to be the stable structure. As discussed above, the calculated intrinsic stacking-fault energy is too large in the MEAM, leading to this result.

The outward relaxation of the top layer for all three surfaces of Si and Ge is a somewhat unphysical result. Further refinements of the Si and Ge MEAM functions will need to be made in order to change the sign of the first-layer interlayer relaxation. We feel that one possiblity is the large value of our stacking-fault energy. The value of the stacking-fault energy is an important part of the energetics of the (111) surface. We should also note that Wilson,[64] using the old uncorrected form of the

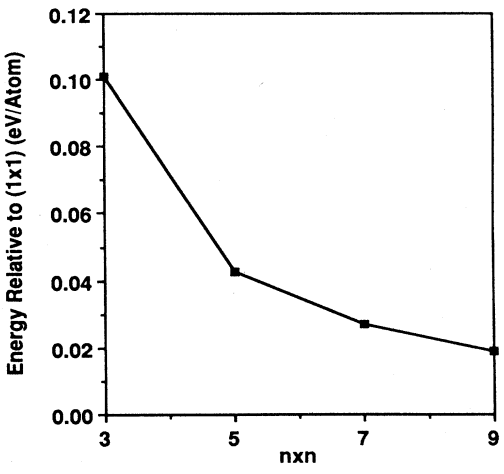

FIG. 7. The surface energies of the relaxed $(n\times n)$ dimer-stacking-fault structures relative to the relaxed (1×1) surface of Si. As a consequence of the large calculated intrinsic stacking-fault energy of Si (see text for more details), the (7×7) is not predicted to be the stable structure.

TABLE VIII. Surface interlayer distances and atomic displacements of the Si(100) (2×1) surface. Figure 6 shows the actual displacements and geometry. Negative z represents relaxation away from the bulk. The ideal Si interlayer distance is 1.357 Å. The LDA values in parentheses are from Ref. 48.

Layer	y (Å)	z (Å)	Interlayer distance (Å)
1	0.438 (0.695)	−0.298 (0.092)	$d_{12}=1.566$
2	0.041 (0.119)	−0.091 (−0.005)	$d_{23}=1.423$
3	0.000 (0.000)	0.033 (−0.130)	$d_{34}=1.372$
4	0.000 (0.000)	0.029 (−0.078)	$d_{45}=1.359$
5	−0.020 (−0.032)	0.004 (0.000)	

TABLE IX. Surface interlayer distances and atomic displacements of the Ge(100) (1×1) surface. The bulk Ge interlayer value is 1.415 Å.

Layer	z (Å)	Interlayer distance (Å)
1	−0.372	$d_{12}=1.749$
2	−0.037	$d_{23}=1.433$
3	−0.019	$d_{34}=1.413$
4	−0.020	$d_{45}=1.413$
5	−0.004	$d_{56}=1.417$

TABLE X. Surface energies for the Si and Ge (110) surfaces. Energies are in eV/(surface atom).

	Si	Ge
Ideal	1.69	1.88
(1×1)	1.30	1.48

TABLE XI. Surface interlayer distances for the relaxed Si and Ge (110) (1×1) surfaces. The bulk interlayer spacings for Si and Ge are 1.919 and 2.000 Å, respectively.

	Interlayer distance (Å)	
	Si	Ge
d_{12}	2.161	2.296
d_{23}	1.936	1.982
d_{34}	1.924	2.022
d_{45}	1.921	2.003

TABLE XII. Surface interlayer distances for the relaxed Si and Ge (111) (1×1) surfaces. The bulk interlayer spacings for the first two layers of Si are 0.79 and 2.35 Å and, for Ge, 0.82 and 2.45 Å. The LDA values in parentheses are from Ref. 63.

	Interlayer distance (Å)	
	Si	Ge
d_{12}	1.084 (0.587)	1.109
d_{23}	2.376 (2.360)	2.462
d_{34}	0.791 (0.746)	0.788
d_{45}	2.354 (2.339)	2.458

MEAM,[7] found Si-surface reconstructions similar to the results presented here.

D. Clusters

There has been a significant amount of recent experimental[65] and calculational[66,67] work on the energetics and structure of small silicon clusters. We report here the results of a few MEAM calculations of these small clusters to see if the new method, which has been fitted to bulk properties, gives a reasonable extrapolation to small clusters where the energy and geometry are known from first-principles calculations. We let the total cluster energy, E_c, be given by

$$E_c = NE_b + N^{2/3}(E_b + E_s) + \cdots \tag{22a}$$

or

$$E_c/N = E_b + N^{-1/3}(E_b + E_s) \cdots , \tag{22b}$$

where E_b (<0) is the bulk energy per atom and E_s (>0) the surface energy of an average surface atom in the cluster.

To facilitate extrapolation to the bulk, we now plot the energy per atom, E_c/N, versus $N^{-1/3}$. In Fig. 8 we compare the results of the energy per atom for small clusters of N atoms that we believe have the lowest energy, i.e., optimized geometry for a specific number of atoms. Finding the appropriate geometry is a nonrivial task for greater than four or so atoms, as there are many nearly equivalent energetic configurations with large barriers separating them. Many different initial geometries were tried and each structure was relaxed. As discussed below, we find a number of metastable cluster geometries sometimes close in energy.

First, consider the curves for the smallest cluster

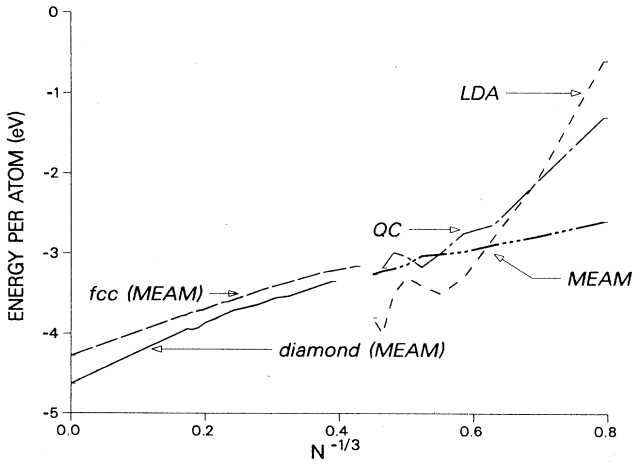

FIG. 8. Energy per atom of silicon clusters as a function of cluster size N. The first-principles calculations—LDA (Ref. 50) and QC (Ref. 51)—of small clusters are compared to MEAM calculations. Energies of the cluster at a global minimum are shown. Also shown are MEAM calculated energies of larger clusters in both the diamond and fcc structures.

($N^{-1/3} > 0.4$). Note that the LDA calculations[66] and the QC calculations[67] differ by as much as ± 1 eV. The MEAM calculations agree reasonably well (± 0.2 eV) with the QC calculations for the larger clusters, but diverge significantly for the very small clusters. (The dimer energy is a factor of 2 too large in the MEAM compared to experiment or the QC calculations.) The MEAM does not show the oscillations of the QC calculations that are necessary to predict the experimentally observed "magic number" cluster stability.[65] The MEAM predicts a dimer bond length of 2.36 Å, in comparison with QC calculations of 2.246 Å. For the trimer, the MEAM predicts an equilateral triangle with a bond length of 2.65 Å as the minimum-energy structure. At only 0.05 eV higher in energy, an isosceles triangle with bond length 2.43 Å and apex angle of 79° exists as a metastable structure. The QC calculations yield an isosceles triangle with bond length 2.165 Å and apex angle of 80°, in reasonable agreement with the metastable structure. For the four-atom cluster, the MEAM predicts a square with a bond length of 2.58 Å, while the QC calculations predict a rhombus with bond length of 2.30 Å. The minimum-energy structure for the five-atom cluster is predicted to be a square with the fifth atom centered above the square. At only 0.03 eV above this structure, a metastable structure of a triangle with atoms above and below the plane of the triangle is found. The out-of-plane bond lengths are calculated to be 2.45 Å. The QC calculations yield this structure as the minimum-energy cluster with a bond length of 2.338 Å. The predicted geometries of the MEAM are in reasonable qualitative agreement with the QC and LDA calculations, but the bond lengths and angles are certainly not in quantitative agreement with the first-principles calculations.

Also shown in Fig. 8 is the MEAM energy of larger clusters based on the diamond and fcc structures. Note that the MEAM predicts the stability of diamond-based packing down to a size of about $N=16$ ($N^{-1/3}=0.4$). We may estimate a surface energy of 1.3 eV/atom from the slope of these curves [see Eq. 22(b)]. This agrees quite well with the surface energies of 0.7–1.8 eV/atom reported in the preceding subsection. The transition from planar to 3D clusters is predicted to be at $N=4-5$, in agreement with the first-principles calculations.[67,68]

In summary, we would caution against the use of the MEAM as presented to calculate details of small silicon clusters. Even though the qualitative behavior is in agreement with first-principles calculations, many details are not. For example, in some cases a metastable cluster is in agreement with QC calculations, while the lowest-energy cluster is not. Further refinement of the method, e.g., fitting to dimer properties, may allow quantitative predictions of small-cluster behavior to be made. On the other hand, the results for the larger clusters seem reasonable and may be used, for example, in kinetic models of growth.

E. Electron-density profiles

In this subsection we compare the electron-density distributions in the Si diamond structure described by the

MEAM expression given in Eq. (13) and one obtained from a first-principles self-consistent pseudopotential (SCP) calculation. Even though in the spirit of the MEAM the electron density is sampled only at the atomic sites, it is nonetheless instructive to examine the spatial features of the electron density described by Eq. (13). In other words, we may consider Eq. (13) to give the atomic density at site i whether or not an atom is present at this site. The details of the SCP method can be found elsewhere;[68] here we will repeat only those details pertinent to our discussion. The calculations are performed within the local-density-functional theory applied in the momentum-space formalism,[68] using *ab initio* pseudopotentials,[69] and the Wigner form of the exchange-correlation potential.[70] The wave functions were expanded, in all cases, in a plane-wave basis set with a constant-energy cutoff of $|\mathbf{K}+\mathbf{G}|^2=11.5$ Ry. During the self-consistency iterations, the charge density was sampled at ten special $\mathbf{k}$ points in the irreducible Brillouin zone; self-consistency iterations were terminated when input and output screening potentials converged to less than 1×10^{-4} Ry. Convergence of our basis set and $\mathbf{k}$-point sampling can be assessed by calculating the total energy and equilibrium lattice constant. The calculations predict a total energy of -7.912 Ry/atom and a lattice constant of 5.45 Å, in good agreement with the theoretical calculations of Yin and Cohen[25] and experiment.[24]

The main modification of the second term in Eq. (13) to the original spherically averaged electron density is to introduce some angular dependence, which can model the covalent bonding or bond-bending forces present in the Si diamond structure. A detailed comparison of the angular dependence of the electron density predicted by the two methods (MEAM and SCP) is obtained by sampling the electron density at a constant distance from a reference atom, along several crystallographic directions. One expects to see the largest charge density along the bonding direction, [111], and the smallest away from the bonded atom, $[\bar{1}\,\bar{1}\,\bar{1}]$. Since the MEAM determines the host density of a given configuration of atoms by computing the electron density of each atom due to its neighbors, we have chosen to look at the angular dependence near a lattice site at 0.5 Å away from a reference atom. This distance is outside the core region where the pseudovalence wave functions are well described.

In Fig. 9 the electron density along different crystallographic directions predicted by the MEAM and SCP methods are compared. Also shown is the electron density that would be obtained by neglecting the angle-dependent term in Eq. (13). For comparison, the electron density for all methods has been normalized to 1 along the [111] direction. Note that for a single-component system the absolute value of the density does not matter, as discussed above in Sec. II. As can be seen in Fig. 9, the trends in the angular variation of the electron density of the MEAM expression [Eq. (13)] are in good agreement with the SCP calculations, although the magnitude of the angular effects is not quite the same. Note that the spherically averaged EAM electron density exhibits essentially no angular variations 0.5 Å away from the reference atom. The MEAM qualitatively reproduces the

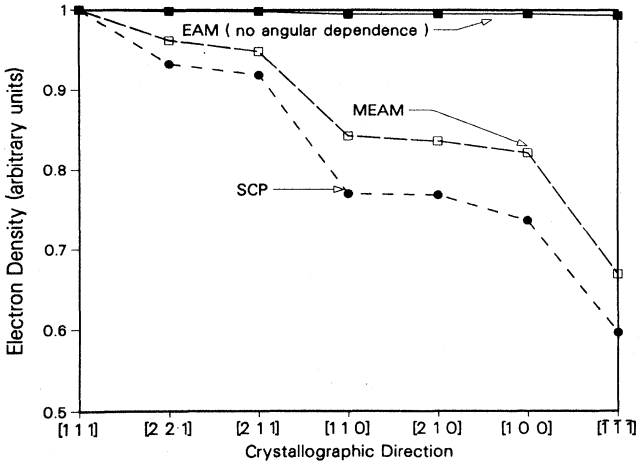

FIG. 9. The electron density along several crystallographic directions in bulk Si calculated with the SCP method and the MEAM [see Eq. (13)]. For both the SCP and MEAM the electron density was sampled at 0.5 Å away from a reference atom, and normalized to 1 along the [111] direction for comparison. The angular variation of the electron density is similar for the two materials.

electron density in bulk Si. With the correct angular variation of the electron density, one would expect that the bond-bending forces, which are obtained by differentiation of Eq. (1) using Eq. (13), are well described. As mentioned earlier, the angular term in Eq. (13) was necessary to obtain the correct value of the Cauchy discrepancy (ΔC). The negative value of ΔC is related to the bond-bending forces.

Another interesting comparison between the MEAM and SCP methods can be made by considering the variation of the electron density at one point along the Si—Si bond as a function of lattice constant. This comparison is shown in Fig. 10. The electron density is sampled 0.5 Å away from a reference atom. With the electron density sampled near the atom, the MEAM reasonably characterizes the electron-density variations for compression of the lattice, while the SCP results exhibit a minimum at the equilibrium lattice constant, rather than a smooth decrease with expansion characterized by the MEAM. The minimum seen in Fig. 10 for the SCP results is directly related to the covalent nature of the Si—Si bond. At the equilibrium lattice constant, the electron density in the center of the bond is a maximum. As the lattice is distorted from equilibrium value, the bond charge decreases, resulting in a redistribution of the electron density out of the center of the bond, back towards the atom. This is the variation seen in Fig. 10 for the SCP results. The MEAM does not allow for the charge redistribution and hence cannot properly characterize this effect.

To better understand the relationship between the covalent bonding and the minimum in electron density in Fig. 10, we have performed similar calculations for the simple metal Na. The variations in the electron density near the Na atom as a function of lattice constant is also

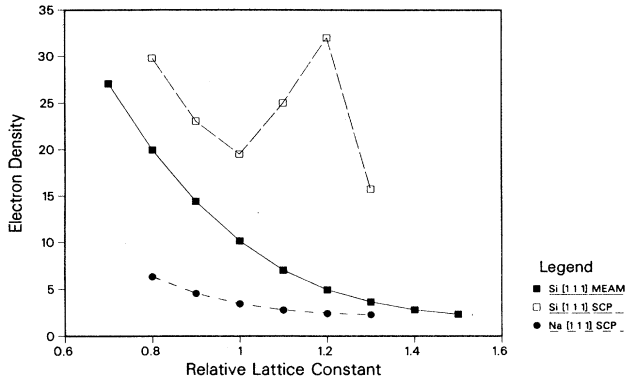

FIG. 10. The variation of the electron density vs relative lattice constant in bulk Si and Na. The electron density (arbitrary units) is samples at 0.5 Å away from a reference atom along the [111] direction. For Si the minimum in the calculated electron density for the SCP method reflects the maximum electron density at the center of the bond at the equilibrium lattice constant. As the lattice constant is changed from the equilibrium value, the charge transfers out of the bond back towards the atom. Also shown is the electron-density variation (sampled at 0.5 Å away from a reference Na atom) vs lattice constant. The difference between the Si and Na curves clearly shows the different behavior for metallic and covalent-bonding systems. Na exhibits no minimum in electron density near the atom at the equilibrium lattice constant. Note that the electron density for Si calculated using the MEAM (arbitrary units) agrees with the SCP calculation for compressed lattices but not for expanded lattices.

given in Fig. 10. For the simple metal Na, we find no minimum in the electron density. A comparison between the Si and Na results clearly points out the intrinsic differences between covalent and metallic bonding. The minimum in the electron density found for the SCP results suggests that the form of the electron density described in Eq. (19) for the MEAM should be further modified to include this effect.

IV. SUMMARY

We have developed the modified EAM, a semiempirical method based on the metallic EAM, to calculate the energetics of covalently bonded silicon, germanium, and their alloys. In order to include the bond-bending forces that manifest themselves in the elastic constants, an angle-dependent electron density has to be used. The new method has been applied to the calculations of bulk structural energies and geometries, point defects, surfaces, and small clusters. In general, there has been reasonable agreement with experimental data and first-principles calculations, but a number of exceptions have been noted that indicate that further refinements of the model are needed. As stated in the Introduction, we wanted to develop a simple universal model for covalent materials. To that end we have made a start, but it is clear that the present model is not adequate to explain quantitatively all of the known experimental and first-principles calculations of Si and Ge. We are actively pursuing further refinements of this material to that end.

ACKNOWLEDGMENTS

The authors would like to acknowledge many valuable discussions with Dr. M. S. Daw, Dr. S. M. Foiles, Dr. C. F. Melius, and Dr. C. M. Rohlfing (of this laboratory), and Professor R. A. Johnson (University of Virginia), without which this work could never have progressed to this point. This work was supported by the Division of Materials Sciences of the Office of Basic Energy Sciences, U.S. Department of Energy.

APPENDIX A

In this appendix we discuss in detail how we calculate the elastic shear constants. The procedure we use is as follows: (1) calculate the energy of a perfect crystal, E_0, periodic in three dimensions; (2) apply a specific strain (discussed below); (3) relax the lattice, keeping the periodic vectors fixed at their strained values to get the relaxed energy, E_1; (4) use the formulas below and the numerically calculated second derivatives of the energy to calculate the elastic constants. [In our previous paper, we neglected the relaxation in step (3).] For the case of γ in diamond this relaxation is nonzero and leads to an important contribution to γ. For γ' in the diamond structure and both shears in structures with one atom per primitive unit cell, there is no relaxation and our previous calculations are correct.

The strains are given by the following transformation:

$$x'=x+\varepsilon y,\quad y'=y,\quad z'=z \quad \text{for } \gamma\ ,$$

$$x'=(1+\varepsilon)x,\quad y'=y/(1+\varepsilon),\quad z'=z \quad \text{for } \gamma'\ .$$

In either case the second energy derivative $E''=2(E_1-E_0)/\varepsilon^2$.

The shear constants are given by

$$\gamma=E''/V \quad \text{and} \quad \gamma'=E''/4V\ ,$$

where V is the volume of the system.

APPENDIX B

The angular term in the host density [Eq. (13)] includes a double summation over atoms. Daw[27] noted that this summation could be replaced by a single summation over atoms. The angular term is reproduced here for convenience:

$$\sum_{\substack{j\ (\neq i),\\ k\ (\neq i)}} [a_j^1 a_k^1 \cos\theta_{jik} - a_j^2 a_k^2 (1-3\cos^2\theta_{jik})]\rho_j^a(R_{ij})\rho_k^a(R_{ik})\ . \tag{B1}$$

The term not involving $\cos\theta$ can easily be rewritten as follows:

$$\left[\sum_{j\ (\neq i)} a_j^2 \rho_j^a(R_{ij})\right]^2 . \tag{B2}$$

In the first term,

$$\cos\theta_{jik}=\frac{R_{ij}\cdot R_{ik}}{|R_{ij}|\,|R_{ik}|}=\frac{\sum_{\alpha} R_{ij}^{\alpha}R_{ix}^{\alpha}}{|R_{ij}|\,|R_{ik}|}\ , \tag{B3}$$

where R_{ij}^{α} ($\alpha=x,y,z$) is the α component of R_{ij}.

The first term can now be rewritten:

$$\sum_{\alpha}\sum_{\substack{j\,(\neq i),\\ k\,(\neq i)}}\left[a_j^1 a_k^1\rho_j^{\alpha}(R_{ij})\rho_k^{\alpha}(R_{ik})\frac{R_{ij}^{\alpha}R_{ik}^{\alpha}}{|R_{ij}|\,|R_{ik}|}\right]=\sum_{\alpha}\left[\sum_{j\,(\neq i)} a_j^1\rho_j^{\alpha}(R_{ij})\frac{R_{ij}^{\alpha}}{|R_{ij}|}\right]^2 . \tag{B4}$$

In the last term,

$$\cos^2\theta_{jik}=\frac{(R_{ij}\cdot R_{ik})^2}{|R_{ij}|^2\,|R_{ik}|^2}=\frac{\left[\sum_{\alpha} R_{ij}^{\alpha}R_{ik}^{\alpha}\right]^2}{|R_{ij}|^2\,|R_{ik}|^2}=\frac{\sum_{\alpha,\beta} R_{ij}^{\alpha}R_{ij}^{\beta}R_{ik}^{\alpha}R_{ik}^{\beta}}{|R_{ij}|^2\,|R_{ik}|^2}\ . \tag{B5}$$

The last term can now be rewritten:

$$3\sum_{\alpha,\beta}\sum_{\substack{j\,(\neq i),\\ k\,(\neq i)}}\left[a_j^2\rho_j^{\alpha}(R_{ij})\frac{R_{ij}^{\alpha}R_{ij}^{\beta}}{|R_{ij}|^2}\right]\left[a_k^2\rho_k^{\alpha}(R_{ij})\frac{R_{ik}^{\alpha}R_{ik}^{\beta}}{|R_{ik}|^2}\right]=3\sum_{\alpha,\beta}\left[\sum_{j\,(\neq i)} a_j^2\rho_j^{\alpha}(R_{ij})\frac{R_{ij}^{\alpha}R_{ij}^{\beta}}{|R_{ij}|^2}\right]^2 . \tag{B6}$$

Thus we have replaced the double summation in Eq. (A1) with the single summations in Eqs. (B2), (B4), and (B6).

---

*Permanent address: Department of Physics, University of California, Davis, CA 95616.

[1]R. Biswas and D. R. Hamann, Phys. Rev. Lett. **55**, 2001 (1985).

[2]F. Stillinger and T. Weber, Phys. Rev. B **31**, 5262 (1985).

[3]J. Tersoff, Phys. Rev. Lett. **56**, 632 (1986); Phys. Rev. B **37**, 6991 (1988); **39**, 5566 (1989); B. W. Dodson, *ibid.* **35**, 2795 (1987).

[4]J. R. Chelikowsky, J. C. Phillips, M. Kamal, and M. Strauss, Phys. Rev. Lett. **62**, 292 (1989).

[5]D. W. Brenner and B. J. Garrison, Phys. Rev. B **34**, 1304 (1986).

[6]E. Pearson, T. Takai, T. Halicioglu, and W. A. Tiller, J. Cryst. Growth **70**, 33 (1984).

[7]M. I. Baskes, Phys. Rev. Lett. **59**, 2666 (1987).

[8]K. E. Khor and S. Das Sarma, Phys. Rev. B **38**, 3318 (1988).

[9]M. S. Daw and M. I. Baskes, Phys. Rev. B **29**, 6443 (1984); Phys. Rev. Lett. **50**, 1285 (1983).

[10]S. M. Foiles, M. I. Baskes, and M. S. Daw, Phys. Rev. B **33**, 7983 (1986).

[11]J. B. Adams, S. M. Foiles, and W. G. Wolfer, J. Mater. Res. **4**, 102 (1989).

[12]S. M. Foiles, Phys. Rev. B **32**, 3409 (1985).

[13]M. S. Daw, Surf. Sci. Lett. **166**, L161 (1986); S. M. Foiles, *ibid.* **191**, L779 (1987); M. S. Daw and S. M. Foiles, Phys. Rev. Lett. **59**, 2756 (1987); B. W. Dodson, Phys. Rev. B **35**, 880 (1987).

[14]S. M. Foiles, Phys. Rev. B **32**, 7685 (1985); in *Computer-Based Microscopic Description of the Structure and Properties of Materials,* Vol. 63 of *Materials Research Society Symposium Proceedings,* edited by J. Broughton, W. Krakow, and S. T. Pantelides (MRS, Pittsburgh, 1985), p. 61; in *Physical and Chemical Properties of Thin Metal Overlayers and Alloy Surfaces,* Vol. 83 of *Materials Research Society Symposium Proceedings,* edited by D. M. Zehner and D. W. Goodman (MRS, Pittsburgh, 1987), p. 175.

[15]S. M. Foiles and M. S. Daw, J. Mater. Res. **2**, 5 (1987).

[16]M. I. Baskes and M. S. Daw, in *Computer Simulation in Materials Science,* Proceedings of the 1986 ASM Materials Science Seminar, edited by R. J. Arsenault, J. R. Beeler, Jr., and D. M. Esterling (American Society for Metals, Metals Park, OH, 1986), p. 137.

[17]M. S. Daw and R. D. Hatcher, Solid State Commun. **56**, 697 (1985); J. S. Nelson, E. C. Sowa, and M. S. Daw, Phys. Rev. Lett. **61**, 1977 (1988); L. Ningsheng, X. Wenlan, and S. C. Shen, Solid State Commun. **67**, 837 (1988).

[18]M. I. Baskes, S. M. Foiles, and M. S. Daw, J. Phys. (Paris) Colloq. **49**, C5-483 (1988).

[19]M. I. Baskes, S. M. Foiles, and C. F. Melius, J. Nucl. Mater. **145-147**, 339 (1987); M. S. Daw and S. M. Foiles, Phys. Rev. B **35**, 2128 (1987).

[20]J. H. Rose, J. R. Smith, F. Guinea, and J. Ferrante, Phys. Rev. B **29**, 1963 (1984).

[21]L. Pauling, *The Nature of the Chemical Bond* (Cornell University Press, Ithaca, NY, 1960).

[22]L. Brewer, Lawrence Berkeley Laboratory Report No. LBL-3720, 1975 (unpublished).

[23]*Smithells Metals Reference Book,* edited by E. A. Bandes (Butterworths, London, 1983).

[24]C. S. Barrett and T. B. Massalski, *Structure of Metals* (McGraw-Hill, New York, 1966).

[25]M. T. Yin and M. L. Cohen, Phys. Rev. B **26**, 5668 (1982); Phys. Rev. Lett. **45**, 1004 (1980).

[26]P. Ho, M. E. Coltrin, J. S. Binkley, and C. F. Melius, J. Phys. Chem. **90**, 3399 (1986); C. F. Melius (private communication).

[27]M. S. Daw, Phys. Rev. B **39**, 7441 (1989); M. S. Daw (private communication).

[28]A. K. Prinja, M. S. Lazo, and M. I. Baskes (unpublished).

[29]L. Kleinman, Phys. Rev. **128**, 2614 (1962).

[30]H. d'Amour, W. Denner, H. Schulz, and M. Caradona, J. Appl. Crystallogr. **15**, 148 (1982).

[31]C. S. G. Cousins, L. Gerward, J. Staun Olsen, B. Selsma, and B. J. Sheldon, J. Appl. Crystallogr. **15**, 148 (1982).

[32]O. H. Nielsen and R. M. Martin, Phys. Rev. B **32**, 3792 (1985).

[33]R. A. Johnson, Phys. Rev. B **39**, 12 554 (1989).

[34]V. T. Bubdik, S. S. Gorelik, A. A. Zaitsev, and A. Y. Polyakov, Phys. Status Solidi B **66**, 427 (1974).

[35]A. Qteish and R. Resta, Phys. Rev. B **37**, 1308 (1988); see also J. L. Martins and A. Zunger, Phys. Rev. Lett. **56**, 1400 (1986).

[36]R. Car, P. J. Kelly, A. Oshiyama, and S. T. Pantelides, Phys. Rev. Lett. **52**, 1814 (1984); **54**, 360 (1985).

[37]G. A. Baraff and M. Schlüter, Phys. Rev. B **30**, 3460 (1984); G. A. Baraff, E. O. Kane, and M. Schlüter, *ibid.* **21**, 5662 (1980).
[38]Y. Bar-Yam and J. D. Joannopoulos, Phys. Rev. B **30**, 1844 (1984).
[39]K. C. Pandey, Phys. Rev. Lett. **75**, 2287 (1986).
[40]G. D. Watkins, in *Lattice Defects in Semiconductors, 1974,* Inst. Phys. Conf. Ser. No. 23, edited by F. A. Huntley (Institute of Physics, London, 1975), p. 1.
[41]*Atomic Diffusion in Semiconductors,* edited by D. Shaw (Plenum, New York, 1973).
[42]G. L. McVayard and A. R. DuCharme, in *Lattice Defects in Semiconductors, 1974,* Ref. 40, p. 91.
[43]M. Hirota, in *Lattice Defects in Semiconductors, 1974,* Ref. 40, p. 164.
[44]R. J. Needs and R. M. Martin, Phys. Rev. B **30**, 5390 (1984).
[45]P. J. H. Denteneer, in *Atomic Scale Calculations in Materials Science,* Vol. 141 of *Materials Research Society Symposium Proceedings,* edited by J. Tersoff, David Vanderbilt, and V. Vitek (MRS, Pittsburgh, 1989), p. 343.
[46]K. E. Khor and S. D. Sarma, Phys. Rev. B **36**, 7733 (1987).
[47]F. F. Abraham and I. P. Batra, Surf. Sci. **163**, L752 (1985).
[48]J. A. Appelbaum and D. R. Hamann, Surf. Sci. **74**, 21 (1978).
[49]D. J. Chadi, Phys. Rev. Lett. **43**, 43 (1979).
[50]M. T. Yin and Marvin L. Cohen, Phys. Rev. B **24**, 2302 (1981).
[51]J. E. Northrup, Phys. Rev. Lett. **54**, 815 (1985).
[52]K. C. Pandey, Phys. Rev. Lett. **47**, 1913 (1981).
[53]R. M. Tromp, R. J. Hamers, and J. E. Demuth, Phys. Rev. Lett. **55**, 1303 (1985).
[54]S. D. Kevan, Phys. Rev. B **32**, 2344 (1985).
[55]J. A. Kubby, J. E. Griffith, R. S. Becker, and J. S. Vickers, Phys. Rev. B **36**, 6079 (1987).
[56]W. R. Lambert, P. L. Trevor, M. J. Cardillo, A. Sakai, and D. R. Hamann, Phys. Rev. B **35**, 8055 (1987).
[57]M. Needels, M. C. Payne, and J. D. Joannopoulos, Phys. Rev. Lett. **58**, 1765 (1987).
[58]M. Needels, M. C. Payne, and J. D. Joannopoulos, Phys. Rev. B **38**, 5543 (1988).
[59]D. J. Chadi, Phys. Rev. B **19**, 2074 (1979).
[60]H. Neddermeyer and St. Tosch, Phys. Rev. B **38**, 5784 (1988).
[61]D. Vanderbilt, Phys. Rev. B **36**, 6209 (1988).
[62]K. Takayanagi, Y. Tanishiro, M. Takahashi, and S. Takahashi, J. Vac. Sci. Technol. A **3**, 1502 (1985); see also Surf. Sci. **164**, 367 (1985).
[63]J. E. Northrup, J. Ihm, and M. L. Cohen, Phys. Rev. Lett. **47**, 1910 (1981).
[64]J. H. Wilson, D. Phil. thesis, Oxford University, 1988.
[65]W. Begemann, S. Dreihöfer, G. Ganteför, H. R. Siekmann, K. H. Meiwes-Broer, and H. O. Lutz, in *Elemental and Molecular Clusters,* edited by T. P. Martin (Springer, New York, in press).
[66]D. Tománek and M. A. Schlüter, Phys. Rev. B **36**, 1208 (1987).
[67]K. Raghavachari and C. M. Rohlfing, J. Chem. Phys. **89**, 2219 (1988), and references therein.
[68]M. Schlüter, J. R. Chelikowsky, S. G. Louie, and M. L. Cohen, Phys. Rev. B **12**, 4200 (1975); J. Ihm, A. Zunger, and M. L. Cohen, J. Phys. C **12**, 4409 (1979); K. C. Pandey, Phys. Rev. Lett. **49**, 223 (1982); I. P. Batra and S. Ciraci, Phys. Rev. B **33**, 4312 (1986).
[69]G. B. Bachelet, D. R. Hamann, and M. Schlüter, Phys. Rev. B **26**, 4199 (1982).
[70]E. Wigner, Phys. Rev. **46**, 1002 (1934).